Journal of Electroceramics (2023) 51:246–257
https://doi.org/10.1007/s10832-023-00333-x

Synthesis techniques and advanced applications of spinel ferrites: A short review

Shayista Gaffar[1] · Amit Kumar[3] · Ufana Riaz[1,2]

Received: 27 May 2023 / Accepted: 5 September 2023 / Published online: 15 September 2023

Abstract
Spinel ferrites are among the most promising soft magnetic materials due to their superior coercivity, tailored band gap, high saturation magnetization, and other physical, thermal, and electrical characteristics. In the areas of cancer treatment, disease detection, magnetic resonance imaging, drug delivery, and release, soft ferrite nanoparticles (SFNPs) offer limitless potential. Ferrite nanoparticles are utilized in electronic domains to create sensors, biosensors, transducers, and transformers. Spinel ferrites are used in the treatment of wastewater, and they can be coupled with other nano materials for photocatalysis and adsorption. In this review, attention has been paid to the synthesis, distinctive characteristics, and various applications of spinel ferrites.

Keywords Spinel ferrites · Photocatalyst, photo-degradation · Wastewater remediation

1 Introduction

Spinel ferrite nanoparticles (SFNPs) have been widely used several applications such as photodegradation of organic pollutants [1–8], gas sensors [9], high-recurrence gadgets [10], and water-splitting [11–13]. SFNPs also are useful in increasing reaction yield, lowering reaction temperatures, and catalyzing certain chemical reactions. Several investigations have been carried out which establish the photocatalytic as well as antibacterial activity of SFNPs [14–18]. Recent research has also proven that Zn (II) substituted cobalt ferrites are more effective in comparison to Mn(II) and Cu(II) substituted cobalt ferrites [19, 20] as antibacterial materials. Due to their low energy band gap, high surface area/volume ratio, and ease of synthesis, SFNPs are viewed as valuable photocatalysts [21–28]. The upcoming section discusses the synthesis techniques employed for designing SFNPs.

✉ Ufana Riaz
ufana2002@yahoo.co.in

1 Materials Research Laboratory, Department of Chemistry, Jamia Millia Islamia, New Delhi 110025, India

2 Department of Chemistry and Biochemistry, North Carolina Central University, Durham, NC 27707, USA

3 Theory & Simulation Laboratory, Department of Chemistry, Jamia Millia Islamia, New Delhi-110025, India

1.1 Structure of spinel ferrite nanoparticles (SFNPs)

SFNPs are metal oxides having a spinel structure with the general formula AB_2O_4, where A and B address different metal cations situated at the tetrahedral (A site) and octahedral (B site). The metal cations are tetrahedrally/octahedrally coordinated to oxygen atoms at both the sites. The physico-chemical properties are significantly impacted by the type, quantity and composition of ferrites [29–31]. On the basis of the distribution of cations at the tetrahedral (A) and octahedral (B) sites, SFs have been classified into three categories; normal spinel ferrites, inverse spinel ferrites and mixed spinel ferrites. In normal SFs, the divalent cations M^{2+}occupy tetrahedral (A) sites while the trivalent cations Fe^{3+} are on octahedral (B) site. The structural formula of such ferrites is $[M^{2+}]_{(A)}[Fe_2{}^{3+}]_{(B)}O_4{}^{2-}$) (for example $ZnFe_2O_4$, $CdFe_2O_4$) [32]. The structure of normal spinel is depicted in Fig. 1 [33].

Inverse spinel ferrites are those that have the trivalent ions evenly distributed between the A and B sites and the divalent ions only on the B site. The standard formula for inverse spinel structure is ($[M^{2+}Fe^{3+}]^{B}$ $[Fe^{3+}]^{A}$ O_4) (for example, $FeOFe_2O_3$, $NiFe_2O_4$, $CuFe_2O_4$ and $CoFe_2O_4$). In this structure, half of the Fe^{3+} ions occupy A-sites while the remaining occupies B-sites [34].

In mixed spinel ferrites, the divalent cations M^{2+} and the trivalent cations Fe^{3+} ions are distributed at both the

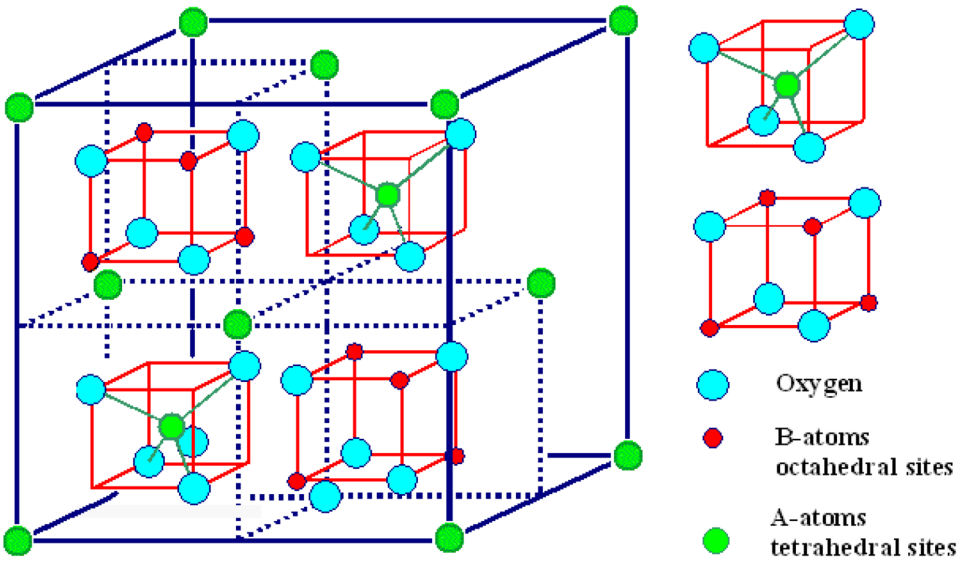

Fig. 1 Structure of spinel ferrite reproduced from reference no [33]

octahedral (B) site and the tetrahedral (A) site (for example $MnFe_2O_4$) [35]. The structure of inverse spinels is illustrated in Fig. 2 [36].

The basic rule to determine whether the structure is normal spinel or inverse spinel can be understood on the basis of crystal field stabilization energy (CFSE) as: For normal spinel's CFSE of B^{+3} ions in Octahedral Field > CFSE of B^{+3} ions in Tetrahedral Field > CFSE of A^{+2} ions in Octahedral Field > CFSE of A^{+2} ions in Tetrahedral Field [i.e. if CFSE of B^{+3} ions in Octahedral Field is largest of all CFSE]. For inverse spinel's CFSE of A^{+2} ions in Octahedral Field > CFSE of A^{+2} ions in Tetrahedral Field > CFSE of B^{+3} ions in Octahedral Field > CFSE of B^{+3} ions in Tetrahedral Field [i.e. if CFSE of A^{+2} ions in Octahedral Field is largest of all CFSE].

2 Synthesis techniques of spinel ferrites (SFs)

SFs are prepared using a variety of methods, including electrochemical, hydrothermal, micro emulsion, sol–gel, hydrothermal, solid-state, sono-chemical, precipitation and template methods. Each of these processes have advantages and limitations of its own which are discussed in the upcoming sections.

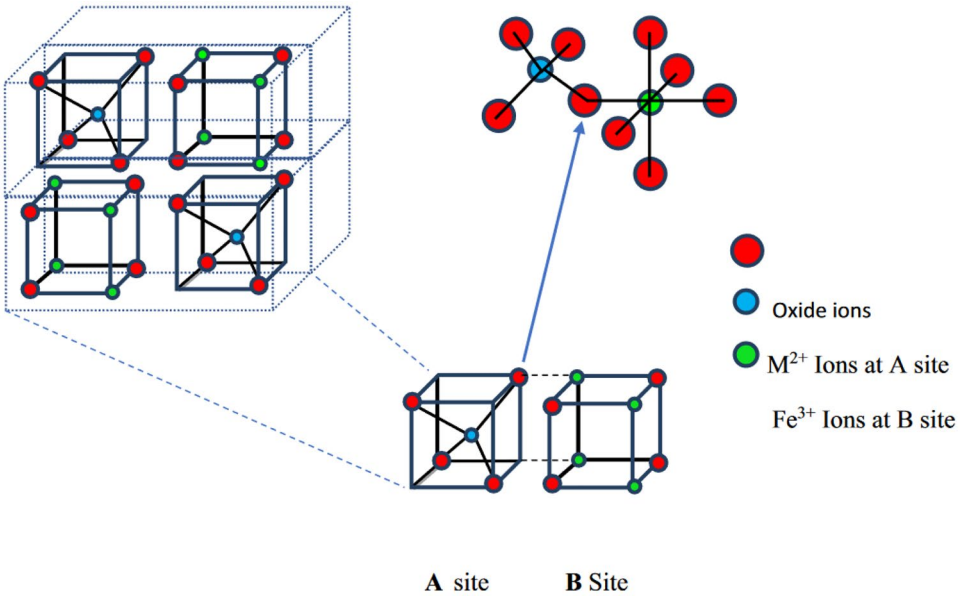

Fig. 2 Structure of Inverse Spinels derived from reference no [36]

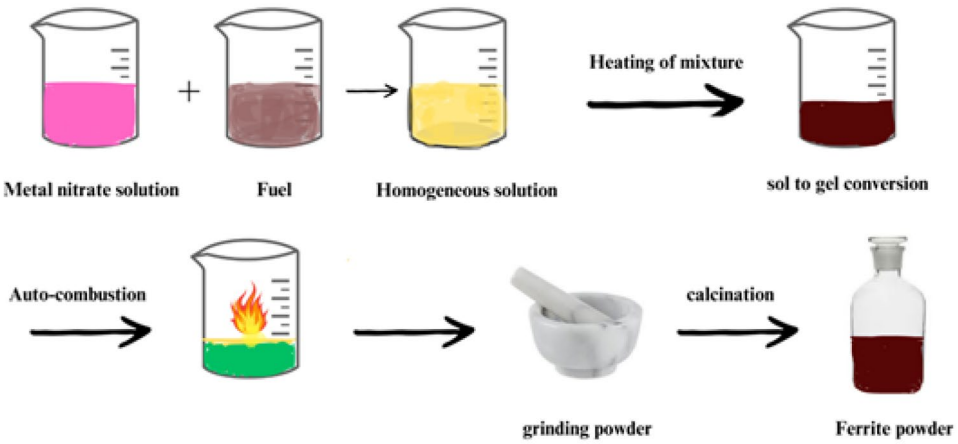

Fig. 3 Schematic representation of synthesis of SFs by Sol-Gel method

2.1 Sol-gel method

Metal alkoxide are utilized in the sol-gel process, which undergo hydrolysis and buildup a gel at room temperature. The sol-gel mixture strategy enjoys a few benefits such as solid stoichiometric control, and lack of utilization of sophisticated modern instruments. It is one of the most widely adopted techniques for controlling the microstructure. It is possible to blend ferrite materials with a restricted size propagation and controlled shape by changing the given temperature in sol-gel somewhere in the range of 25 °C - 200 °C. The sol-gel approach is utilized to synthesize simple spinel ferrites such as $CuFe_2O_4$, $ZnFe_2O_4$, $NiFe_2O_4$, $CdFe_2O_4$ [28]. The sintering temperature, sintering time, and addition of dopants impact the physicochemical properties of spinel ferrites, Fig. 3.

2.2 Co-precipitation method

This is one of the oldest methods to obtain spinel ferrites. The arrangement in this approach contains a combination of divalent and trivalent progress metals in a mole proportion of 1:2. As a source of trivalent metal particles, dissolvable salts containing Fe (III) are regularly used, and the test is normally completed in a basic media. To produce high-quality ferrite materials, the synthesis procedure demands precise pH adjustment and which is commonly provided by Ammonium or sodium hydroxide solutions. The solution is then vigorously stirred or agitated in the absence or presence of heat under inert conditions. To obtain phase pure ferrites, the resultant powder must be annealed at various temperatures ranging from 500 to 100 °C, Fig. 4 [37].

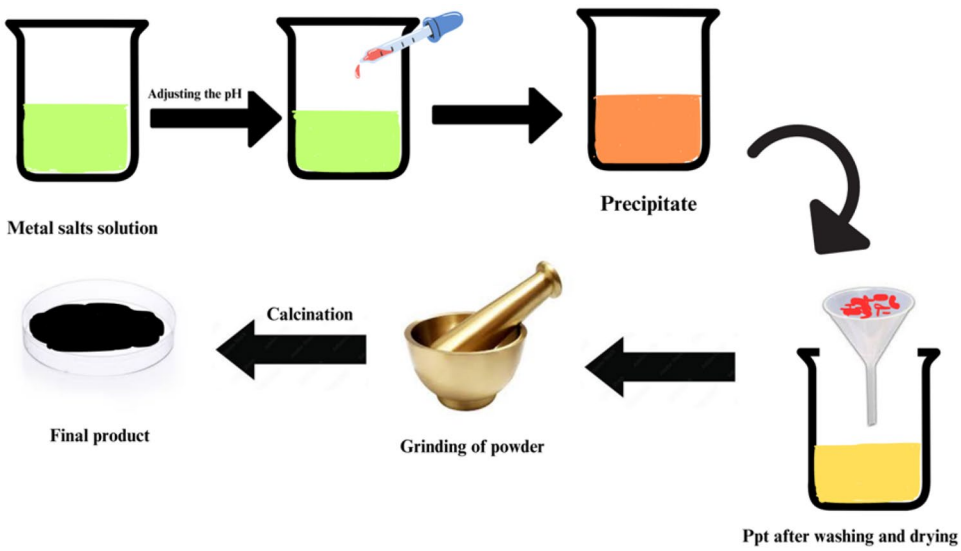

Fig. 4 Schematic representation of synthesis of SFs by precipitation method

2.3 Hydrothermal method

The hydrothermal method is one of the ecofriendly and promising synthesis methods available for the synthesis of SFs. In this method an iron salt such as $Fe(NO_3)_3.9H_2O$/ $FeCl_3.6H_2O$, and a salt of the metal is used, commonly $M(NO_3)_2$, MSO_4, or MCl_2. Depending on the type of metal salt being used, salts are dissolved in water or another solvent while being stirred, and the pH is then adjusted to a range between 7 and 12. The mixture is heated for 12 to 24 h in an autoclave before naturally cooling to room temperature. Followed by washing and filtration or centrifugation to obtain the solid, it is then overnight dried at around 85 °C. The precursor chemicals are pulverized collectively in a ball-mill for mechano-thermal treatment, rather than dissolving. The Fe (III) salt is added to a metal oxide (M_2O_3) seed when using seed-hydrothermal procedures. The identical process as previously described above is followed while heating the two compounds in an autoclave, Fig. 5 [38].

2.4 Solvo-thermal method

The solvothermal method is utilized to make ferrite materials with enhanced physical and chemical properties, which can be used in biomedical applications. In order to facilitate the interaction of precursors during synthesis, the procedure uses a solvent under moderate to high pressure (usually between 1 atm and 10,000 atm) and temperature (generally between 100 °C and 1000 °C). Fluid or non-watery solvents can be used to deliver ferrite materials with accurate command over size dispersion, shape, and glasslike progressively works in the solvothermal process. Certain trial factors, like reaction temperature, reaction duration, solvent, surfactant, and antecedents, can be changed to differ these actual highlights. Utilizing the solvothermal combination process, the no of ferrite materials and composites have been made, Fig. 6 [39].

2.5 Micro- emulsion method

In this method small modification to the synthesis conditions easily produces nanoparticles with a restricted size distribution and size control. The three components of this method—water, oil, and surfactant allow for the control of a number of parameters, including particle size, geometry, morphology, homogeneity, and surface area [40]. It usually involves two sub-methods one utilizing oil/water and other water/oil. In both cases surfactants are used always in concentration which is above the critical micelle concentration (CMC).

2.6 Comparison of synthesis methods

There are also large number of methods available that are utilized in the synthesis of SFs, like sono-chemical[41], electro-chemical, [42], and microwave assisted method [43]. The properties of SFs are strongly dependent upon the method utilized for the synthesis, thus preparation method can be selected on the basis of desired application. Every method has its set of advantages and disadvantages.

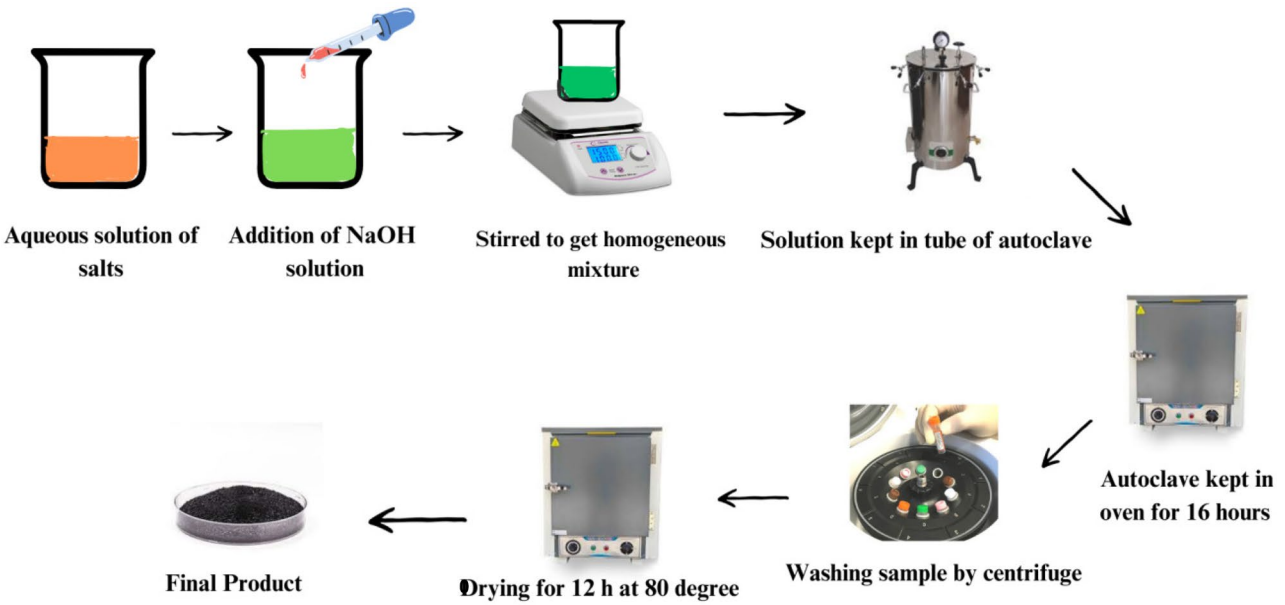

Fig. 5 Schematic representation of synthesis of SFs by hydrothermal method

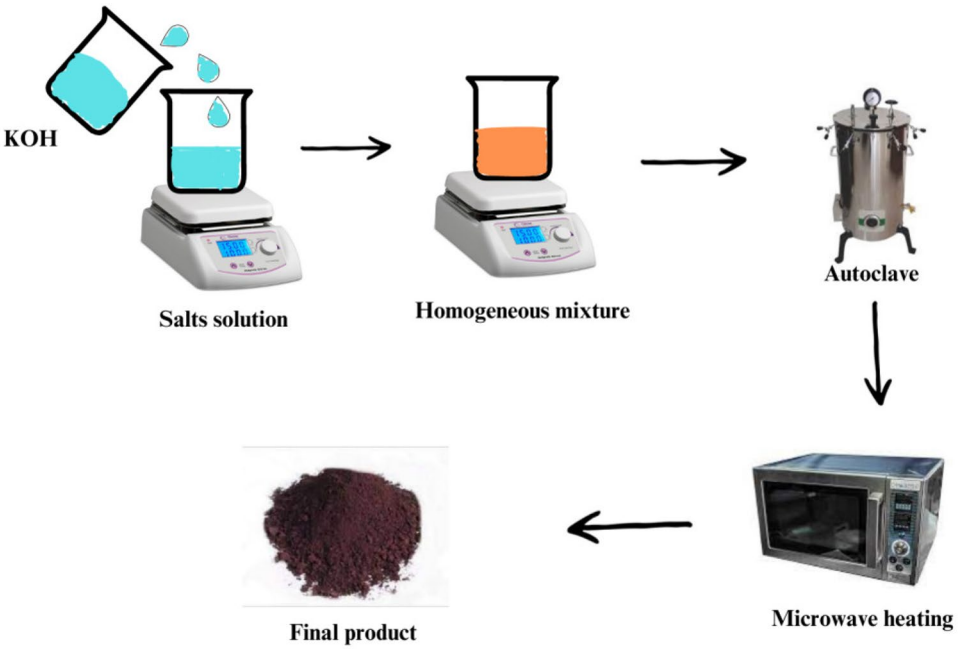

Fig. 6 Schematic representation of synthesis of SFs by Solvothermal method

The advantages and disadvantages of various synthesis methods are shown in Table 1.

3 Techniques adopted for characterizing SFNPs

Understanding and surveying the results of SFNPs requires an exhaustive investigation of their physico-chemical features. There are different ways for describing FNPs, each with different set of information and nature of data, for example: X-ray diffraction (XRD), Raman spectroscopy (RS), atomic force microscopy (AFM), transmission electron microscopy (TEM), scanning electron microscopy (SEM), vibrating sample magnetometer (VSM), superconducting quantum interference device (SQUID), Fourier transform infrared (FT-IR) spectroscopy, Energy-dispersive X-ray spectroscopy (EDS), X-ray photoelectron spectroscopy(XPS), thermogravimetric Analysis (TGA) [44–48].

3.1 Size and shape

FNP's size and shape are the main qualities that decide their strength and attractive properties [49]. Further developed approaches are expected to decide the exact size of SFNPs, particularly those under 20 nm [50]. For deciding the size and state of SFNPs, number of approaches has been explored.

Table 1 Advantages and disadvantages of different routes of synthesis of SFs

Method	Advantages	Disadvantages
Sol–Gel	Low cost as compared to conventional processes, producing high quality materials, homogeneity and purity at low temperature, control over textures, size and surface properties, high quality, production of materials with large surface area.	Long processing time, low yield, difficult to avoid residual porosity.
Co- Precipitation	Pure and homogeneous material, complete precipitation of metal ions, materials of higher surface area can be synthesized.	Large time consumption, impurity formation, probability, can be affected by several factors like pH, temp, ionic strength.
Hydrothermal	One step synthetic procedure, environment friendliness, good dispersion.	High cost equipment, high pressure, high temp.
Solvothermal	Ease of synthesis, composition control, high surface area and dispersion.	Need expensive autoclaves, safety issues, impossibility of observing reaction process.
Micro emulsion	Control of particle properties, reduced waste, time and cost saving, improved safety aspects.	Require large amount of surfactants, less yield, temperature dependent. -

The most well-known procedures are high-resolution transmission electron microscopy (HRTEM) and field emission scanning electron microscopy (FE-SEM). The fundamental way of operation of nanoparticles can be understood utilizing these strategies. Scherer's condition is utilized to compute the size of SFNPs from XRD diffraction. TEM results provide size affirmation, Fig. 7 [51]. X-ray photoelectron spectroscopy, Mossbauer spectroscopy, and dynamic light scattering (DLS) are a section of different strategies used to decide mean molecule size.TEM estimations of Fe_3O_4

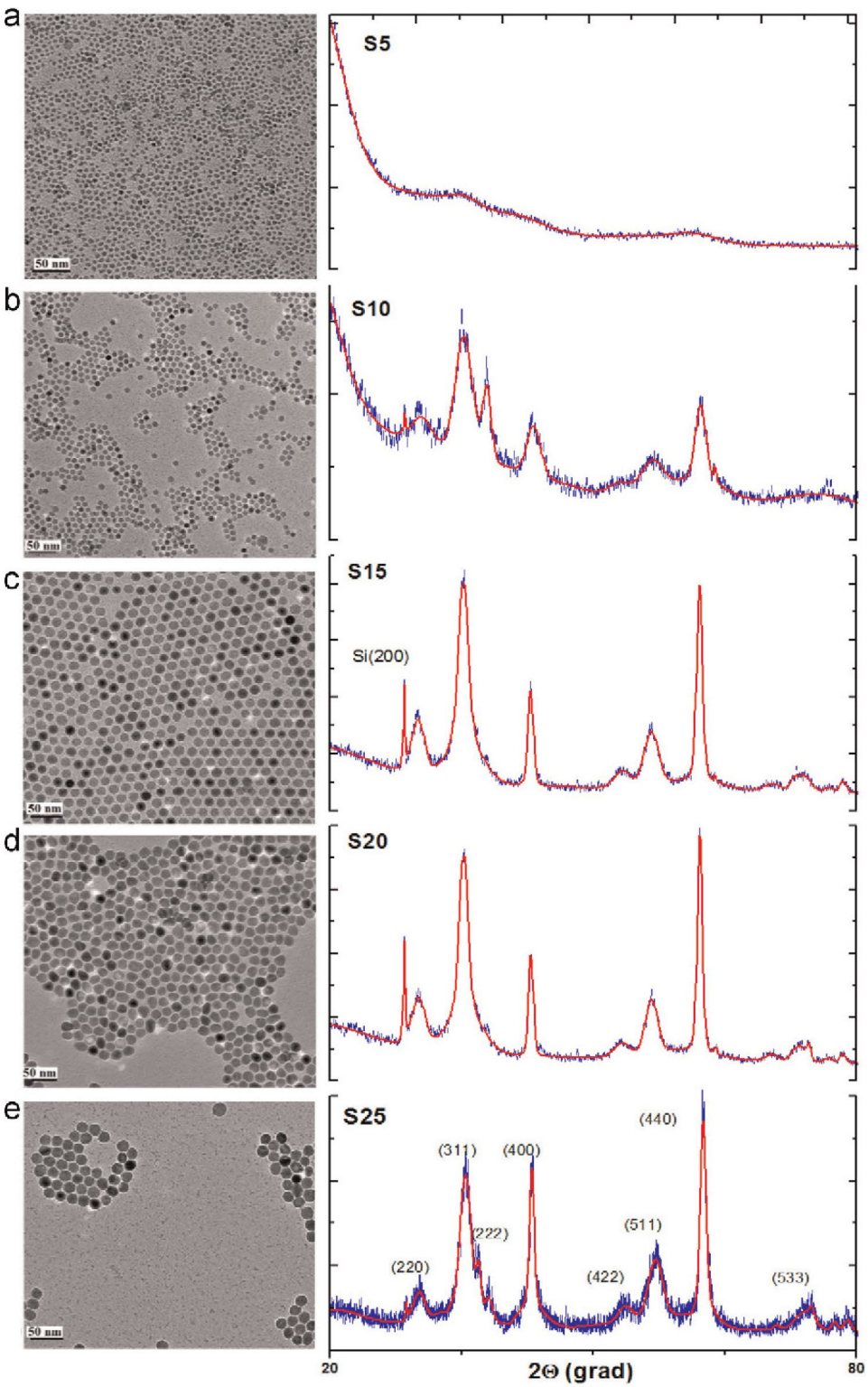

Fig. 7 TEM pictures and XRD examples of Fe_3O_4 NPs with size 5–15 nm (Reproduced from Ref. [51], Copyright 2015, Elsevier)

and Fe_3O_4-alpha-olefin sulphonate (AOS) NPs, for instance, uncovered normal sizes of 10 nm -20 nm and 5 nm -10 nm, which were in agreement with the DLS studies, Fig. 8 [52].

3.2 Elemental and mineral composition

Inductively coupled plasma mass spectrometry (ICP-MS) can be utilized to decide the basic composition of SFNPs with more accuracy and recognition limits [53, 54]. ICP-OES and atomic absorption spectroscopy (AAS) are also utilized for exploring the compositions of SFNPs.

3.3 Structure and bonding

XPS, FT-IR, TGA, Raman spectroscopy (RS), and X-beam absorption spectroscopy are some of the known strategies used to research primary and promising properties. (XAS), XPS and FT-IR are utilized to determine the foundation of metal–oxygen bonds, providing recognizable proof of the presence of spinel structure as well as the presence of other substances adsorbed on the outer layer of particles. The oxidation state, restricting energy, and essential substance of materials on a superficial level can be generally resolved utilizing XPS. Figure 9 shows the XPS spectra of Fe_3O_4, $MnFe_2O_4$ and $CoFe_2O_4$ [25]. The zeta potential Fig. 9(a), of $CoFe_2O_4$ is similar to that of Fe_3O_4, but $MnFe_2O_4$ showed higher value than Fe_3O_4. The XRD patterns of $MnFe_2O_4$, $CoFe_2O_4$ and Fe_3O_4 were indexed to spinel ferrites, and Fe_3O_4 to cubic crystalline bulk magnetite. The XPS profiles show that the surface molar ratio of Fe/Mn or Fe/Co for $MnFe_2O_4$, $CoFe_2O_4$ are 2:1, in accordance with the metal ion ratio taken in solution. The remanence magnetization values of $MnFe_2O_4$, $CoFe_2O_4$ and Fe_3O_4 were 3.49, 8.46 and 0.70 emu/g, while maximal saturation magnetization of $MnFe_2O_4$, $CoFe_2O_4$ and Fe_3O_4 were 32.02, 46.99 and 55.41 emu/g respectively.

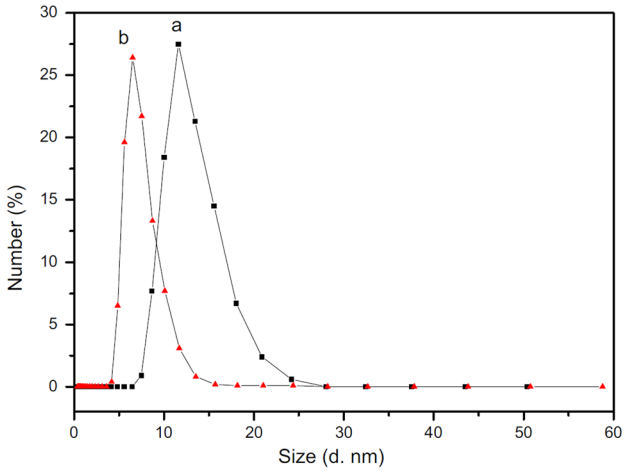

Fig. 8 DLS estimations of: (**a**) unadulterated Fe_3O_4 NPs and, (**b**) Fe_3O_4-AOS NPs covered with twofold layered AOS. (Ref. [52], Copyright 2015, Elsevier)

The FT-IR spectra of $NiFe_2O_4$, $CoFe_2O_4$ and $ZnFe_2O_4$ is shown in Fig. 10 [55]. The spectra shows metal–oxygen stretching vibration from the tetrahedral site to be around 584–540 cm^{-1} range and for the octahedral site to be in the range of 397–389 cm^{-1}.

3.4 Surface morphology

AFM, TEM, and SEM could be utilized to operate the surface morphology of SFNPs. These techniques are normally used to imagine and quantify the state of nanoparticles. TEM, specifically, is a more adaptable procedure for getting substance, morphological, and crystallite data on FNPs [56]. It can convey more prominent goal down to the nuclear level. TEM can make nuclear scale basic guides for compositional investigation when utilized related to other spectroscopic instruments like EDS and electron energy loss spectroscopy (EELS), Fig. 11(a-e) [57].

3.5 Magnetic measurements

EPR, VSM, and SQUID are popular techniques used to examine and measure the magnetic characteristics of SFNPs. EPR is a delicate procedure for detecting and identifying free radicals and paramagnetic centers in chemicals and chemical processes, such as the F-center. When high sensitivity magnetization measurements are necessary, VSM and SQUID are used, especially because VSM's sensitivity limit is around 106 emu [58].

3.6 Properties of Spinel Ferrites

On the basis of distribution and nature of the cations on the tetrahedral (A) and octahedral (B) sites, SFs can be divided into different catogeries as: paramagnetic, diamagnetic, ferromagnetic, ferrimagnetic, antiferromagnetic, and superparamagnetic [59]. Superparaamagnetic nanoparticles are very useful in wastewater treatment. Superparaamagnetism is observed in small ferro and ferri magnetic nanomaterials (3–50 nm) [60].The spinel ferrites usually have low band gap energy values which makes them suitable for processes like photocatalysis [61].Spinel ferrites are widely used at microwave frequencies because they have low electrical conductivities when compared to other magnetic materials. These materials are typically semiconductors with conductivities between 10^2 and 10^{-11} Ω^{-1} cm^{-1}.

4 Photocatalytic applications of SFNPs

The presence of various toxins in modern wastewater release is an overall concern. Harmful natural poisons like colors, phenols, chloro-phenols, and nitro-phenols have for quite some time been an issue to treat and eliminate, particularly when presented to visible light. A few results have shown

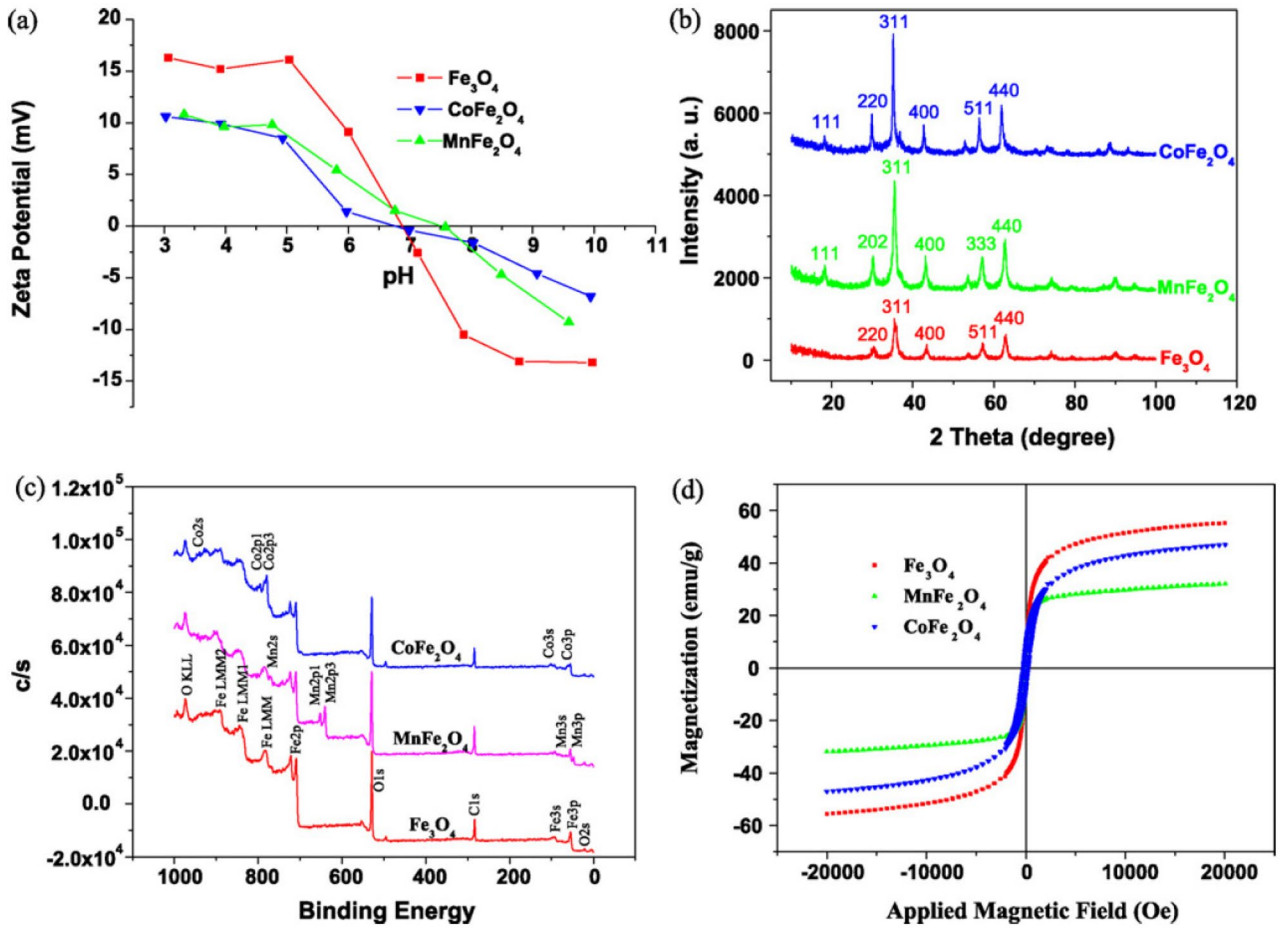

Fig. 9 (**a**) Zeta potential as a function of pH; (**b**) X-ray diffraction pattern; (**c**) wide XPS scan; and (**d**) VSM curves of Fe_3O_4, $MnFe_2O_4$, and $CoFe_2O4$ MNPs. (Ref. [25], Copyright 2010, Elsevier)

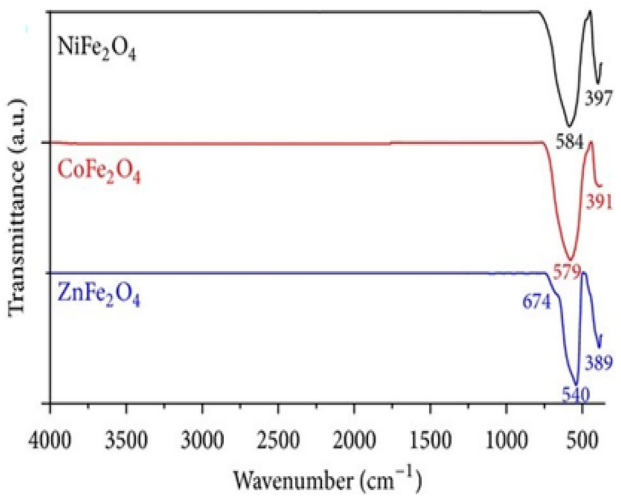

Fig. 10 IR Spectra of $NiFe_2O_4$, $CoFe_2O_4$ and $ZnFe_2O_4$ reproduced from Reference no [55]

that these pollutants can be eliminated using SFNPs as photocatalyst, and it is one of most extensively investigated area of research [61–64]. SFNPs incorporate their capacity to work as a photocatalyst (without adjustment), in composites (surface covered with semiconductors), and within the sight of oxidants like H_2O_2. Under visible light, an electron (e) is stimulated from the valence band (VB) to the conduction band (CB) of SFNPs leaving a hole (h^+). At the CB (**reaction** 1), the deposited e^- is successfully polished off by separated oxygen gas present in the water [65, 66].The hole (h^+) created by photolytic exposure joins with water to deliver vigorous hydroxyl free radicals (**reaction** 3). The contaminants are in closeness to the vigorous radicals because of the great adsorption limit of SFNPs, and are hence immediately gone after by hydroxyl radicals framed on the outer layer of the photocatalyst, (**reaction** 4) [66]. The degraded fragments are then desorbed from the ferrite surface regions. Figure 12 shows a schematic of the process of photocatalysis.

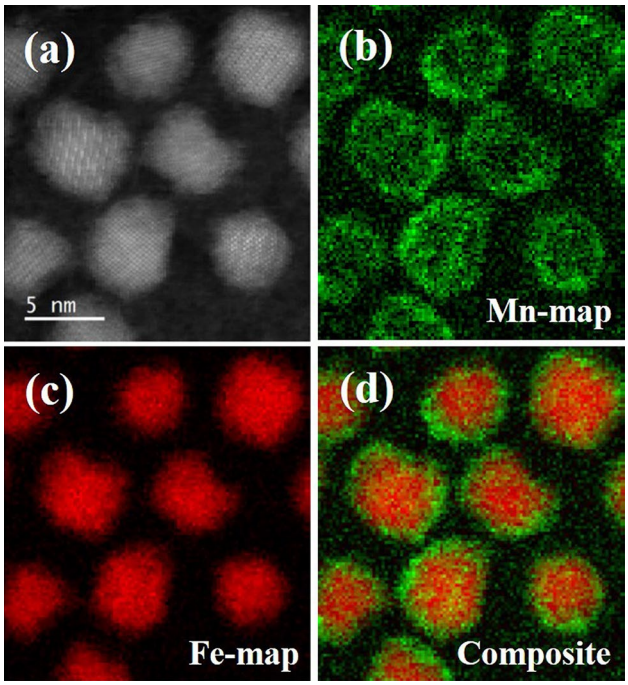

Fig. 11 (**a**) HAADF-STEM images of nanoparticles showing spinel structure in magnetite cores. (**b**) integrated map of the Mn L2,3 EELS signal, where green intensity shows the Mn distribution. (**c**) integrated map of the Fe L2,3 EELS signal, where red intensity shows the Fe distribution. (**d**) Composite image showing Fe-rich core and Mn-rich shell in the nanoparticles

$$e^- + O_2 \rightarrow O_2^{\bullet -} \quad (1)$$

$$O_2^{\bullet -} - + 2H^+ + 2e^- \rightarrow {}^{\bullet}OH + OH^- \quad (2)$$

$$h^+ + H_2O \rightarrow {}^{\bullet}OH + H^+/OH^{\bullet} \quad (3)$$

$$^{\bullet}OH + \text{Organic contaminant (OC)} \rightarrow CO_2(g) + H_2O(1) \quad (4)$$

$$e^- + OC \rightarrow OC^- \rightarrow \text{degradation products} \quad (5)$$

$$h^+ + + OC \rightarrow OC+ \rightarrow \text{degradation products} \quad (6)$$

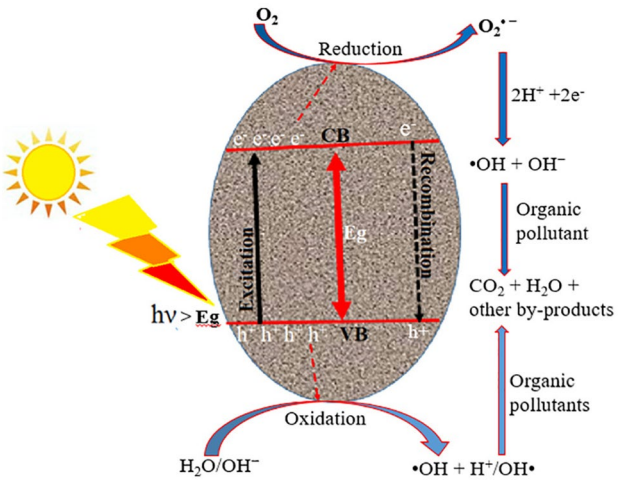

Fig. 12 Schematic outline showing the arrangement of receptive oxygen and hydroxyl extremist under apparent light illumination of semiconductor or ferrite-semiconductor composite, connection with natural contaminations and conceivable corruption items

It is reported that Fe_3O_4@SiO_2 NCs, work as a Fenton-like impetus for the breakdown of H_2O_2 and bring about a high pace of discoloration of MB at neutral pH [67]. In another work, high strength of Fe_3O_4@TiO_2 was seen with close to 100% MB degradation following 5 min of H_2O_2 dilution without any UV illumination [68]. $MnFe_2O_4$/GSC and $MnFe_2O_4$/BT NCs were utilized to photo catalytically degrade ampicillin (AMP) and oxy antibiotic medication (OTC). About 96- and 83%-AMP degradation and 99% and 90% OTC degradation was achieved following 60 and 120 min, respectively [69]. The photocatalytic movement of pyrrole engraved $CoFe_2O_4$/MWCNTs NCs for the degradation of 2-mercaptobenzothiazole was explored in another review [70]. Xiong et al. [71] coordinated CdSZnFe_2O_4(0.10) (CdS-with 10% ZnFe_2O_4) and CdSCoFe_2O_4(0.05) and assessed their photocatalytic impact on RhB degradation. 80% of RhB was degraded using the SFNPs but only 30% of RhB was disintegrated during the third cycle, showing an impressive drop in photocatalytic action. Figure 13(a), (b) shows the schematic of RhB degradation using SFNP.

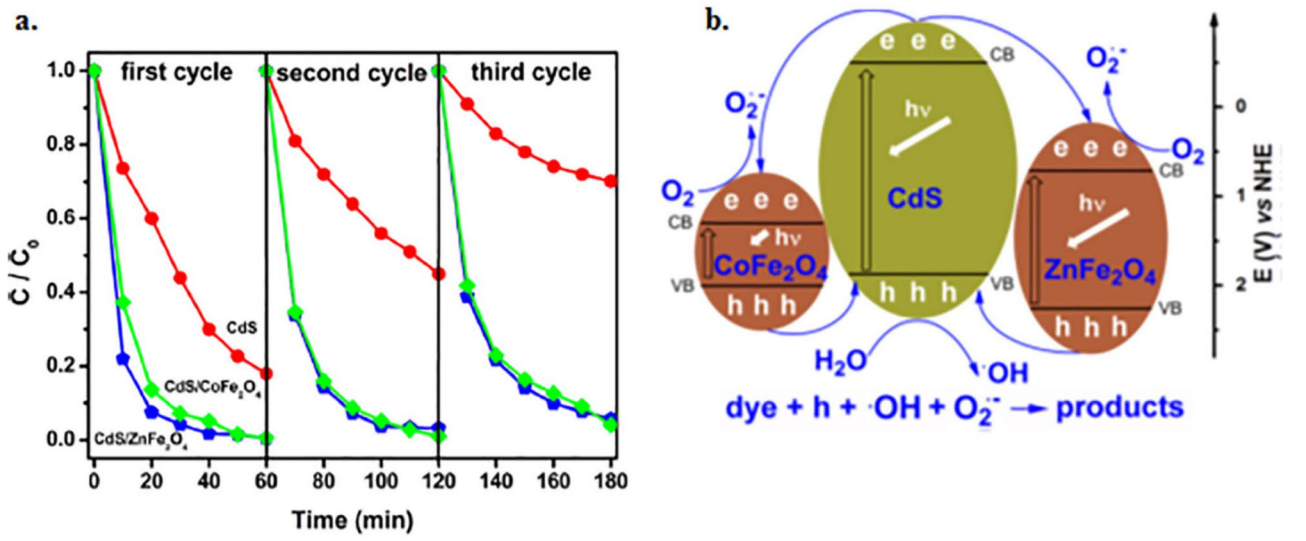

Fig. 13 (**a**) Recyclability of CdS, CdS-$ZnFe_2O_4$(0.10), and CdS-$CoFe_2O_4$(0.05) for three cycles, (**b**) photocatalytic action of the SFNPs (Reproduced from ref. [71])

5 Conclusion

The review highlights the synthesis and photocatalytic applications of SFNPs. On account of their low energy band gap, remarkable magnetic properties, they are utilized in various applications. The diversity in ferrite group nanoparticles can accommodate various elements in different oxidation states which are outstanding and industrially beneficial. There is scope for improvement in the synthesis strategies which can increase the diverse applications of these materials besides photocatalysis. These nanomaterials serve as good research niche for further applications in a variety of organic catalytic processes.

Acknowledgements One of the co-authors Dr. Amit Kumar would like to acknowledge UGC-BSR (project no F-30/569/2021 (BSR)) and DST -SERB SRG/2021/001709 for financial assistance.

Author contributions Ufana Riaz conceptualized the work and Shayista Gaffar wrote the draft article which was edited by Dr. Amit Kumar.

Research data policy and data availability statements The research data is not generated in this review article but deals with reported data.

Declarations

Ethics approval The work is in compliance with ethical standards.

Competing interests The authors declare no competing interests.

References

1. U. Riaz, S. Gaffar, K. Hauser, F. Yan, Visible-light induced degradation of diphenyl urea and polyethylene using polythiophene decorated $CuFe_2O_4$ nanohybrids. Sci. Rep. **13**, 4975 (2023)
2. J. Zia, U. Riaz, Studies on the spectral, morphological and magnetic properties of PCz-PPy copolymer encapsulated $BaFe_2O_4$ nanohybrids. J. Mater. Sci. Mater. Elect. **31**, 22856–22865 (2020)
3. U. Riaz, S.M. Ashraf, J. Kashyap, Enhancement of photocatalytic properties of transitional metal oxides using conducting polymers: A mini review. Mater. Res. Bull. **71**, 75–90 (2015)
4. U. Riaz, S.M. Ashraf, E.S. Aazam, Microwave-assisted catalytic activity of superparamagnetic spinel ferrites. J. Chem. Technol. Biotechnol. **96**(10), 2792–2801 (2021)
5. U. Riaz, S.M. Ashraf, R. Raza, K. Kohli, J. Kashyap, Sonochemical Facile Synthesis of Self-Assembled Poly(*o*-phenylenediamine)/Cobalt Ferrite Nanohybrid with Enhanced Photocatalytic. Ind. Eng. Chem. Res. **55**, 6300–6309 (2016)
6. J. Zia, M. Riyazuddin, E.S. Aazam, U. Riaz, Rapid catalytic degradation of amoxicillin drug using $ZnFe_2O_4$/PCz nanohybrids under microwave irradiation. Mater. Sci. Engg. B **261**, 114713 (2020)
7. J. Zia, S.M. Farhat, E.S. Aazam, U. Riaz, Highly efficient degradation of metronidazole drug using $CaFe_2O_4$/PNA nanohybrids as metal-organic catalysts under microwave irradiation. Env. Sci. Poll. Res. **28**, 4125–4135 (2021)
8. J. Zia, E.S. Aazamand U. Riaz, Facile synthesis of MnO_2 nanorods and $ZnMn_2O_4$ nanohexagons: a comparison of microwave-assisted catalytic activity against 4-nitrophenol degradation, J. Mater. Res. Technol. **9**(5), 9709–9719 (2020)
9. A. Šutka, K.A. Gross, Spinel ferrite oxide semiconductor gas sensors. Sens. Actuators B Chem. **222**, 95–105 (2016)
10. K.L. Routray, S. Saha, D. Behera, Green synthesis approach for nano sized CoFe2O4 through aloe vera mediated sol-gel auto combustion method for high frequency devices. Mater. Chem. Phys. **224**, 29–35 (2019)

11. J.L. Domínguez-Arvizu, J.A. Jiménez-Miramontes, J.M. Salinas-Gutiérrez, M.J. Meléndez-Zaragoza, A. López-Ortiz, V. Collins-Martínez, Study of NiFe2O4 nanoparticles optical properties by a six-flux radiation model towards the photocatalytic hydrogen production. Int. J. Hydrogen Energy. **44**, 12455–12462 (2019)
12. M.T.M. Pendergast, J.M. Nygaard, A.K. Ghosh, E.M.V. Hoek, Using nanocomposite materials technology to understand and control reverse osmosis membrane compaction. Desalination **261**, 255–263 (2010)
13. Q.H. Ng, J.K. Lim, A.L. Ahmad, B.S. Ooi, S.C. Low, Magnetic nanoparticles augmented composite membranes in removal of organic foulant through magnetic actuation. J. Memb. Sci. **493**, 134–146 (2015)
14. M. Munoz, Z.M. de Pedro, J.A. Casas, J.J. Rodriguez, Preparation of magnetite-based catalysts and their application in heterogeneous Fenton oxidation – A review. Appl. Catal. B Environ. **176–177**, 249–265 (2015)
15. P. Hu, M. Long, Cobalt-catalyzed sulfate radical-based advanced oxidation: A review on heterogeneous catalysts and applications. Appl. Catal. B Environ. **181**, 103–117 (2016)
16. M. Anjum, R. Miandad, M. Waqas, F. Gehany, M.A. Barakat, Remediation of wastewater using various nano-materials. Arab. J. Chem. **12**, 4897–4919 (2019)
17. G. Li, X. Nie, Y. Gao, T. An, Can environmental pharmaceuticals be photocatalytically degraded and completely mineralized in water using g-C3N4/TiO2 under visible light irradiation?—Implications of persistent toxic intermediates. Appl. Catal. B Environ. **180**, 726–732 (2016)
18. S. Dabagh, S.A. Haris, Y.N. Ertas, Synthesis, Characterization and Potent Antibacterial Activity of Metal-Substituted Spinel Ferrite Nanoparticles. J. Clust. Sci. **34**, 2067–2078 (2023)
19. M.I.A.A. Maksoud, G.S. El-Sayyad, A.H. Ashour, A.I. El-Batal, M.A. Elsayed, M. Gobara, A.M. El-Khawaga, E.K. Abdel-Khalek, M.M. El-Okr, Antibacterial, antibiofilm, and photocatalytic activities of metals-substituted spinel cobalt ferrite nanoparticles. Microb. Pathog. **127**, 144–158 (2019)
20. M.I.A. Abdel Maksoud, G.S. El-Sayyad, A.H. Ashour, A.I. El-Batal, M.S. Abd-Elmonem, H.A.M. Hendawy, E.K. Abdel-Khalek, S. Labib, E. Abdeltwab, M.M. El-Okr, Synthesis and characterization of metals-substituted cobalt ferrite [Mx Co(1-x) Fe2O4; (M = Zn, Cu and Mn; x = 0 and 0.5)] nanoparticles as antimicrobial agents and sensors for Anagrelide determination in biological samples. Mater. Sci. Eng. C. **92**, 644–656 (2018)
21. G. Mamba, A. Mishra, Advances in Magnetically Separable Photocatalysts: Smart, Recyclable Materials for Water Pollution Mitigation, Catalysts. 6 (2016) 79. [34]B.F.G. Johnson, Nanoparticles in Catalysis. Top. Catal. **24**, 147–159 (2003)
22. J. Govan, Y. Gun'ko, Recent Advances in the Application of Magnetic Nanoparticles as a Support for Homogeneous Catalysts. Nanomaterials. **4**, 222–241 (2014)
23. M.B. Gawande, Y. Monga, R. Zboril, R.K. Sharma, Silica-decorated magnetic nanocomposites for catalytic applications. Coord. Chem. Rev. **288**, 118–143 (2015)
24. J.G. Parsons, M.L. Lopez, J.R. Peralta-Videa, J.L. Gardea-Torresdey, Determination of arsenic(III) and arsenic(V) binding to microwave assisted hydrothermal synthetically prepared Fe3O4, Mn3O4, and MnFe2O4 nanoadsorbents. Microchem. J. **91**, 100–106 (2009)
25. S. Zhang, H. Niu, Y. Cai, X. Zhao, Y. Shi, Arsenite and arsenate adsorption on coprecipitated bimetal oxide magnetic nanomaterials: MnFe2O4 and CoFe2O4. Chem. Eng. J. **158**, 599–607 (2010)
26. S. Verma, D. Verma, A.K. Sinha, S.L. Jain, Palladium complex immobilized on graphene oxide–magnetic nanoparticle composites for ester synthesis by aerobic oxidative esterification of alcohols. Appl. Catal. A Gen. **489**, 17–23 (2015)
27. R.B. Nasir Baig, R.S. Varma, Magnetic Silica-Supported Ruthenium Nanoparticles: An Efficient Catalyst for Transfer Hydrogenation of Carbonyl Compounds. ACS Sustain. Chem. Eng. **1**, 805–809 (2013)
28. A. Hussain, T. Abbas, S.B. Niazi, Preparation of Ni1−Mn Fe2O4 ferrites by sol–gel method and study of their cation distribution. Ceram. Int. **39**, 1221–1225 (2013)
29. V. Kusigerski, E. Illes, J. Blanusa, S. Gyergyek, M. Boskovic, M. Perovic, V. Spasojevic, Magnetic properties and heating efficacy of magnesium doped magnetite nanoparticles obtained by co-precipitation method. J. Magn. Magn. Mater. **475**, 470–478 (2019)
30. T. Tatarchuk, M. Bououdina, W. Macyk, O. Shyichuk, N. Paliychuk, I. Yaremiy, B. Al-Najar, M. Pacia, Structural, Optical, and Magnetic Properties of Zn-Doped CoFe2O4 Nanoparticles. Nanoscale Res. Lett. **12**, 141 (2017)
31. D.H.K. Reddy, Y.-S. Yun, Spinel ferrite magnetic adsorbents: Alternative future materials for water purification? Coord. Chem. Rev. **315**, 90–111 (2016)
32. S. Chandrasekaran, C. Bowen, P. Zhang, Z. Li, Q. Yuan, X. Ren, L. Deng, Spinel photocatalysts for environmental remediation, hydrogen generation, CO 2 reduction and photoelectrochemical water splitting. J. Mater. Chem. A. **6**, 11078–11104 (2018)
33. B. Issa, I. Obaidat, B. Albiss, Y. Haik, Magnetic Nanoparticles: Surface Effects and Properties Related to Biomedicine Applications. Int. J. Mol. Sci. **14**, 21266–21305 (2013)
34. M. Manjunatha, G. Srinivas Reddy, R. Damle, K.J. Mallikarjunaiah, K.P. Ramesh, Estimation of structural composition of the inverse spinel ferrites using 57Fe-Zero Field Nuclear Magnetic Resonance. Ceram. Int. **45**, 9245–9253 (2019)
35. F.G. da Silva, J. Depeyrot, A.F.C. Campos, R. Aquino, D. Fiorani, D. Peddis, Structural and Magnetic Properties of Spinel Ferrite Nanoparticles. J. Nanosci. Nanotechnol. **19**, 4888–4902 (2019)
36. R. Jain, A Review on the Development of XRD in Ferrite Nanoparticles. J. Supercond. Nov. Magn. **35**, 1033–1047 (2022)
37. I.H. Gul, W. Ahmed, A. Maqsood, Electrical and magnetic characterization of nanocrystalline Ni–Zn ferrite synthesis by co-precipitation route. J. Magn. Magn. Mater. **320**, 270–275 (2008)
38. E. Casbeer, V.K. Sharma, X.-Z. Li, Synthesis and photocatalytic activity of ferrites under visible light: A review. Sep. Purif. Technol. **87**, 1–14 (2012)
39. J. Wang, F. Ren, R. Yi, A. Yan, G. Qiu, X. Liu, Solvothermal synthesis and magnetic properties of size-controlled nickel ferrite nanoparticles. J. Alloys Cmpds. **479**(1–2), 791–796 (2009)
40. Z. Enlei, W. Jiaoyi, W. Guosheng, Z. Bengui, X. Yingpeng, Efficient Fenton Oxidation of Congo Red Dye by Magnetic $MgFe_2O_4$ Nanorods. J. Nanosci. Nanotechnol. **16**, 4727–4732 (2016)
41. M.A. Almessiere, Y. Slimani, S. Guner, M. Sertkol, A. Demir Korkmaz, S.E. Shirsath, A. Baykal, Sonochemical synthesis and physical properties of $Co_{0.3}Ni_{0.5}Mn_{0.2}EuxFe_{2-x}O_4$ nano-spinel ferrites. Ultrason. Sonochem. **58**, 104654 (2019)
42. J.G. Ovejero, A. Mayoral, M. Cañete, M. García, A. Hernando, P. Herrasti, Electrochemical Synthesis and Magnetic Properties of MFe 2 O 4 (M = Fe, Mn Co, Ni) Nanoparticles for Potential Biomedical Applications. J. Nanosci. Nanotechnol. **19**, 2008–2015 (2019)
43. N. Kasapoglu, A. Baykal, Y. Koseoglu, M. Toprak, Microwave-assisted combustion synthesis of CoFe2O4 with urea, and its magnetic characterization. Scr. Mater. **57**, 441–444 (2007)
44. S. Singamaneni, V.N. Bliznyuk, C. Binek, E.Y. Tsymbal, Magnetic nanoparticles: recent advances in synthesis, self-assembly and applications. J. Mater. Chem. **21**, 16819 (2011)
45. Y. Ju-Nam, J.R. Lead, Manufactured nanoparticles: An overview of their chemistry, interactions and potential environmental implications. Sci. Total Environ. **400**, 396–414 (2008)
46. L.H. Reddy, J.L. Arias, J. Nicolas, P. Couvreur, Magnetic Nanoparticles: Design and Characterization, Toxicity and

Biocompatibility, Pharmaceutical and Biomedical Applications. Chem. Rev. **112**, 5818–5878 (2012)
47. R.E. El-Shater, H. El Shimy, S.A. Saafan, M.A. Darwish, D. Zhou, A.V. Trukhanov, S.V. Trukhanov, F. Fakhry, Synthesis, characterization, and magnetic properties of Mn nanoferrites. J. Alloys Compd. **928**, 166954 (2022)
48. K.R. Hurley, H.L. Ring, H. Kang, N.D. Klein, C.L. Haynes, Characterization of Magnetic Nanoparticles in Biological Matrices. Anal. Chem. **87**, 11611–11619 (2015)
49. B. Kong, Z.W. Li, L. Liu, R. Huang, M. Abshinova, Z.H. Yang, C.B. Tang, P.K. Tan, C.R. Deng, S. Matitsine, Recent progress in some composite materials and structures for specific electromagnetic applications. Int. Mater. Rev. **58**, 203–259 (2013)
50. S. Lee, X. Bi, R.B. Reed, J.F. Ranville, P. Herckes, P. Westerhoff, Nanoparticle Size Detection Limits by Single Particle ICP-MS for 40 Elements. Environ. Sci. Technol. **48**, 10291–10300 (2014)
51. R. Gabbasov, M. Polikarpov, V. Cherepanov, M. Chuev, I. Mischenko, A. Lomov, A. Wang, V. Panchenko, Mössbauer, magnetization and X-ray diffraction characterization methods for iron oxide nanoparticles. J. Magn. Magn. Mater. **380**, 111–116 (2015)
52. H. Li, L. Qin, Y. Feng, L. Hu, C. Zhou, Preparation and characterization of highly water-soluble magnetic Fe_3O_4 nanoparticles via surface double-layered self-assembly method of sodium alpha-olefin sulfonate. J. Magn. Magn. Mater. **384**, 213–218 (2015)
53. R. Galindo, E. Mazario, S. Gutiérrez, M.P. Morales, P. Herrasti, Electrochemical synthesis of NiFe2O4 nanoparticles: Characterization and their catalytic applications. J. Alloys Compd. **536**, S241–S244 (2012)
54. S. Fernández-Trujillo, N. Rodríguez-Fariñas, M. Jiménez-Moreno, R.D. Martín-Doimeadios, Speciation of platinum nanoparticles in different cell culture media by HPLC-ICP-TQ-MS and complementary techniques: A contribution to toxicological assays. Anal. Chim. Acta. **1182**, 338935 (2021)
55. P. Samoila, C. Cojocaru, I. Cretescu, C.D. Stan, V. Nica, L. Sacarescu, V. Harabagiu, Nanosized Spinel Ferrites Synthesized by Sol-Gel Autocombustion for Optimized Removal of Azo Dye from Aqueous Solution. J. Nanomater. **2015**, 1–13 (2015)
56. H. Lee, T.-H. Shin, J. Cheon, R. Weissleder, Recent Developments in Magnetic Diagnostic Systems. Chem. Rev. **115**, 10690–10724 (2015)
57. D. Samuel, O.A. Abdelgawad, C. Moya, S.M. Vasey, D. Kepaptsoglou, V.K. Lazarov, R.F.L. Evans, D. Meilak, E. Skoropata, J. Lierop, I.H. Isaak, H. Pan, Y. Ijiri, K.L. Krycka, J.A. Borchers, S.A. Majetich, Spin canting across core/shell Fe_3O_4/$MnxFe_{3-x}O_4$ nanoparticles. Sci. Rep. **8**, 3425 (2018)
58. A. Vedrtnam, K. Kalauni, S. Dubey, A. Kumar, A comprehensive study on structure, properties, synthesis and characterization of ferrites. AIMS Mater. Sci. **7**, 800–835 (2020)
59. A. Soufi, H. Hajjaoui, R. Elmoubarki, M. Abdennouri, S. Qourzai, N. Barka, Spinel ferrites nanoparticles: Synthesis methods and application in heterogeneous Fenton oxidation of organic pollutants – A review. Appl. Surf. Sci. Adv. **6**, 100145 (2021)
60. Y.P. Yew, K. Shameli, M. Miyake, N.B.B. Ahmad Khairudin, S.E.B. Mohamad, T. Naiki, K.X. Lee, Green biosynthesis of superparamagnetic magnetite Fe3O4 nanoparticles and biomedical applications in targeted anticancer drug delivery system: A review. Arab. J. Chem. **13**, 2287–2308 (2020)
61. S. Latif, A. Liaqat, M. Imran, A. Javaid, N. Hussain, T. Jesionowski, M. Bilal, Development of zinc ferrite nanoparticles with enhanced photocatalytic performance for remediation of environmentally toxic pharmaceutical waste diclofenac sodium from wastewater. Environ. Res. **216**, 114500 (2023)
62. M. Demirelli, E. Karaoglu, A. Baykal, H. Sozeri, M-hexaferrite–APTES/Pd(0) Magnetically Recyclable Nano Catalysts (MRCs). J. Inorg. Organomet. Polym. Mater. **23**, 1274–1281 (2013)
63. R. Dom, R. Subasri, K. Radha, P.H. Borse, Synthesis of solar active nanocrystalline ferrite, MFe_2O_4 (M: Ca, Zn, Mg) photocatalyst by microwave irradiation. Solid State Commun. **151**, 470–473 (2011)
64. S. Singh, S. Singhal, Transition metal doped cobalt ferrite nanoparticles: Efficient photocatalyst for photodegradation of textile dye. Mater. Today Proc. **14**, 453–460 (2019)
65. M.A. Henderson, A surface science perspective on TiO_2 photocatalysis. Surf. Sci. Rep. **66**, 1 (2011)
66. T.K. Tseng, Y.S. Lin, Y.J. Chen, H. Chu, A Review of Photocatalysts Prepared by Sol-Gel Method for VOCs Removal. Int. J. Mol. Sci. **11**, 2336–2361 (2010)
67. S.-T. Yang, W. Zhang, J. Xie, R. Liao, X. Zhang, B. Yu, R. Wu, X. Liu, H. Li, Z. Guo, Fe_3O_4 @SiO_2 nanoparticles as a high-performance Fenton-like catalyst in a neutral environment. RSC Adv. **5**, 5458–5463 (2015)
68. M. Abbas, B.P. Rao, V. Reddy, C. Kim, Fe_3O_4/TiO_2 core/shell nanocubes: Single-batch surfactantless synthesis, characterization and efficient catalysts for methylene blue degradation. Ceram. Int. **40**, 11177–11186 (2014)
69. S. Gautam, P. Shandilya, B. Priya, V.P. Singh, P. Raizada, R. Rai, M.A. Valente, P. Singh, Superparamagnetic $MnFe_2O_4$ dispersed over graphitic carbon sand composite and bentonite as magnetically recoverable photocatalyst for antibiotic mineralization. Sep. Purif. Technol. **172**, 498–511 (2017)
70. Z. Lu, M. He, L. Yang, Z. Ma, L. Yang, D. Wang, Y. Yan, W. Shi, Y. Liu, Z. Hua, Selective photodegradation of 2-mercaptobenzothiazole by a novel imprinted $CoFe_2O_4$ /MWCNTs photocatalyst. RSC Adv. **5**, 47820–47829 (2015)
71. P. Xiong, J. Zhu, X. Wang, Cadmium Sulfide-Ferrite Nanocomposite as a Magnetically Recyclable Photocatalyst with Enhanced Visible-Light-Driven Photocatalytic Activity and Photostability. Ind. Eng. Chem. Res. **52**, 17126–17133 (2013)